This problem can now be recognised as Görtler's (1954) diverging flow problem which he has subsequently solved and there is no necessity to go into any further detail.

Before we can attempt to solve the second order inviscid flow problem we must specify the outward normal velocity of the inviscid core. This condition can be obtained by once again making use of van Dyke's matching principle, i.e. a 1-term inner expansion must match with a 2-term outer expansion. (In this case the inner expansion is the boundary layer expansion while the outer expansion is the inviscid expansion.) (For details see Appendix C).

The boundary condition turns out to be

$$\hat{\phi}_1 (\hat{r},1) = - \lim_{x \to \infty} [x\Phi_{ox} - \Phi_o] \quad \text{for } \hat{r} > 1 \qquad (3\text{-}22)$$

or in terms of Görtler's variables

$$\hat{\phi}_1 (r,1) = - \frac{(2\xi)^{\frac{1}{2}}}{\hat{r}} \lim_{\eta \to \infty} [\eta F\eta - F] \qquad (3\text{-}23)$$

The second order inviscid problem can now be formulated as

$$\hat{\nabla}^2 \hat{\phi}_1 = 0 \qquad (3\text{-}24)$$

with boundary conditions (3-23) and (3-4).

(Note we have made use of the fact that the first order problem is irrotational.)

Region 2 (the Downstream Region)

As the flow proceeds downstream the boundary layers will tend to meet when $\hat{r} \sim 0$ $(\sqrt{Re})$ i.e. $L \sim \sqrt{Re}$. This means that the second order inviscid problem will become singular and a new expansion must be found. To determine this expansion we define the following downstream variables

$$\overset{*}{r} = \frac{r}{h\sqrt{Re}} \quad , \qquad \overset{*}{z} = \hat{z} \qquad (3\text{-}25)$$

From the dimensional analysis we anticipate that the downstream expansion will be of the following form

$$\hat{\phi} \sim Re^{-\frac{1}{2}} \overset{*}{\phi}_o + Re^{-1} \overset{*}{\phi}_1 + \dots \qquad (3\text{-}26)$$

while the limit process is

$$\lim_{Re \to \infty} \hat{\phi}\,(\overset{*}{r},\overset{*}{z}) \text{ keeping } \overset{*}{r} \text{ and } \overset{*}{z} \text{ fixed} \qquad (3\text{-}27)$$

Proceeding as before we obtain the following first order approximation for the downstream region

$$\left[\overset{*}{\phi}_{o\overset{*}{z}} \left(\frac{\partial}{\partial \overset{*}{r}} - \frac{1}{\overset{*}{r}}\right) - \left(\overset{*}{\phi}_{o\overset{*}{r}} + \frac{1}{\overset{*}{r}}\overset{*}{\phi}_o\right) \frac{\partial}{\partial \overset{*}{z}}\right] \frac{\partial^2 \overset{*}{\phi}_o}{\partial \overset{*}{z}^2} = \frac{\partial^4 \overset{*}{\phi}_o}{\partial \overset{*}{z}^4} \qquad (3\text{-}28)$$

This is identical to the boundary layer equation for region 1 except that the pressure distribution in this case is unknown. Since equation (3.28) is parabolic in $\overset{*}{r}$ it is necessary to specify some initial conditions besides the usual no-slip conditions. This condition is at the moment unknown but can be determined by matching the downstream expansion with the upstream expansion, i.e. the 1-term downstream expansion must match with the 1-term upstream expansion. The initial condition turns out to be (for details see Appendix C)

$$\overset{*}{\phi}_o \left(\frac{1}{\sqrt{Re}}, \overset{*}{z}\right) = \overset{*}{z} \qquad (3\text{-}29)$$

Equation (3.29) states that the initial condition is dependent on the Reynolds number which implies that the velocity profiles will not have similarity features. Intuitively this is what we would expect since at high Reynolds numbers the flow will separate from the disks and then reattach further downstream. At low Reynolds numbers, however, the acceleration effect of the growing boundary layers will be dominant, which in turn will have a favourable effect on the adverse pressure gradient and separation may then not occur. Note that since equation (3.28) will, for large $\overset{*}{r}$, tend asymptotically to

$$\frac{\partial^4 \overset{*}{\phi}_o}{\partial \overset{*}{z}^4} = 0 \qquad (3\text{-}30)$$

it is not necessary to match equation (3-28) with the outer expansion, i.e. region 3. In any event equation (3-28) can now be solved either numerically or else by assuming a series solution. We have chosen the former since most series solutions either diverge or break down at a separation point. The numerical method used was similar to that of Bodoia and Osterle (1961) and has the advantage that the finite difference equations are stable for negative velocities and hence it was possible to integrate through a region of reverse flow. The details of this method are given in appendix D.

<u>Region 3 (the Outer Region)</u>

The outer variables for region 3 are

$$\rho = \frac{r}{hRe} \quad , \quad \hat{z} = \hat{z} \quad , \tag{3-31}$$

The equation of motion in terms of (3-31) becomes

$$\left[\hat{\phi}_{\hat{z}}\left(\frac{\partial}{\partial \rho} - \frac{1}{\rho}\right) - \left(\hat{\phi}_{\rho} + \frac{1}{\rho}\hat{\phi}\right)\frac{\partial}{\partial \rho}\right] \hat{\nabla}^2 \hat{\phi} = \hat{\nabla}^4 \hat{\phi} \tag{3-32}$$

where $$\hat{\nabla}^2 = \frac{1}{Re^2}\left(\frac{\partial}{\partial \rho^2} + \frac{1}{\rho}\frac{\partial}{\partial \rho} - \frac{1}{\rho^2}\right) + \frac{\partial^2}{\partial \hat{z}^2}$$

A certain amount of trial and error suggest that the outer expansion has the following form

$$\hat{\phi} \sim \frac{1}{Re}\psi_o + \frac{1}{Re^2}\psi_1 + \frac{1}{Re^3}\psi_2 + \ldots . \tag{3-33}$$

Substituting (3-33) into (3-32) and applying the outer limit defined as

$$\lim_{Re \to \infty} \hat{\phi}(\rho, \hat{z}) \text{ with } \rho \text{ and } \hat{z} \text{ fixed} \tag{3-34}$$

we obtain the following relationships for $\psi_o$, $\psi_1$ and $\psi_2$

$$\psi_o(\rho,\hat{z}) = F_o(\hat{z})/\rho \qquad (3\text{-}35)$$

where $F_o(\hat{z}) = 1{,}5\ (\hat{z} - \frac{\hat{z}^3}{3})$

$$\psi_1(\rho,\hat{z}) = F_1(\hat{z})/\rho^3 \qquad (3\text{-}36)$$

where $F_1(\hat{z}) = \frac{-9}{840}(\hat{z}^7 - 7\hat{z}^5 + 11\hat{z}^3 - 5\hat{z})$

and $\psi_2(\rho,\hat{z}) = F_2(\hat{z})/\rho^5 \qquad (3\text{-}37)$

where $F_2(\hat{z}) = \frac{-54}{840}[\frac{1}{165}\hat{z}^{11} - \frac{5}{63}\hat{z}^9 + \frac{9}{20}\hat{z}^7 - \frac{11}{20}\hat{z}^5$
$+ 0{,}2864\ \hat{z}^3 + 0{,}38830\ \hat{z}]$

It should be pointed out that higher order terms, i.e. $O(\frac{1}{Re^4})$, are not simply powers of $\rho$ but will in general be complicated functions of the form

$$\psi_3(\rho,\hat{z}) = F_3(\hat{z})\ /G(\rho) \qquad (3\text{-}38)$$

Making use of (3-35), (3-36) and (3-37) it is possible to rewrite the outer expansion as

$$\phi \sim \frac{1}{Re\rho}F_o(\hat{z}) + \frac{1}{Re^2\rho^3}F_1(\hat{z}) + \frac{1}{Re^3\rho^5}F_2(\hat{z}) + \ldots. \qquad (3\text{-}39)$$

It can be seen that this expansion is not uniformly valid for all $\rho$, in fact the expansion breaks down when

$$\frac{Re\rho}{Re^2\rho^3} \sim O(1) \qquad (3\text{-}40)$$

i.e. $\rho \sim \frac{1}{\sqrt{Re}}$

or $\hat{r} \sim O(\sqrt{Re})$

## 3.2 RESULTS AND DISCUSSION

For convenience we now summarise in Table 1 the various expansions and scalings necessary to analyse flow between parallel disks as a parameter perturbation problem.

The asymptotic expansions for the various regions are compared for a range of Reynolds numbers in Figure 3. In each case the normalised centre velocity is plotted against the radial co-ordinate. We argued earlier that the outer expansions would become singular when $\rho$ was $O(\frac{1}{\sqrt{Re}})$ or $\hat{r}$ was $O(Re^{\frac{1}{2}})$. This is confirmed in Figure 3: the singularity causes the outer expansion to deviate quite substantially from the downstream expansion when $\hat{r}$ is less than $\sqrt{Re}$. In Figure 3, two effects are discernible in the entrance region:

(a) the acceleration effect due to the growing boundary layers, and

(b) the deceleration effect caused by the increasing cross-sectional area.

Depending on the relative magnitude of these effects various phenomena occur. At low Reynolds numbers, i.e. low volumetric flow rates, the deceleration effect is small and, therefore, near the entrance the predominant feature is the acceleration of the inviscid core. However, as the Reynolds number is increased the deceleration effect becomes more and more important until it completely swamps the acceleration of the core and there is then a net decrease in the magnitude of the velocity from the entrance. If the Reynolds number is increased even further the one-term downstream expansion approaches (near the entrance) the one-term upstream expansion. (See Figure 4.) This is to be expected since the displacement thickness of the boundary layers diminishes as $Re^{-\frac{1}{2}}$ and subsequently the second order term in the upstream expansion, which takes displacement effects into account, becomes negligible.

In Figure 5 the pressure distribution for the downstream expansion is compared with the pressure distribution computed from

Table 1 - Variables for the different expansions

| Region | r | z | Expansion |
|---|---|---|---|
| I Inviscid | $\hat{r} = r/h$ | $\hat{z} = z/h$ | $\hat{\phi} \sim \hat{\phi}_o + Re^{-\frac{1}{2}} \hat{\phi}_1 + \ldots.$ |
| I Boundary Layer | $\hat{r} = r/h$ | $x = Re^{\frac{1}{2}} (z-1)$ | $\hat{\phi} \sim Re^{-\frac{1}{2}} \phi_o + Re^{-1} \phi_1 + \ldots.$ |
| 2 | $\overset{*}{r} = r/h\sqrt{Re}$ | $\overset{*}{z} = z/h$ | $\hat{\phi} \sim Re^{-\frac{1}{2}} \overset{*}{\phi}_o + Re^{-1} \overset{*}{\phi}_1 + \ldots.$ |
| 3 | $\rho = r/hRe$ | $\hat{z} = z/h$ | $\hat{\phi} \sim Re^{-1} F_o(\hat{z})/\rho + Re^{-2} F_1(\hat{z})/\rho^3$ $+ Re^{-3} F_2(\hat{z})/\rho^5 + \ldots.$ |

Figure 3 - Centre line velocities for various expansions

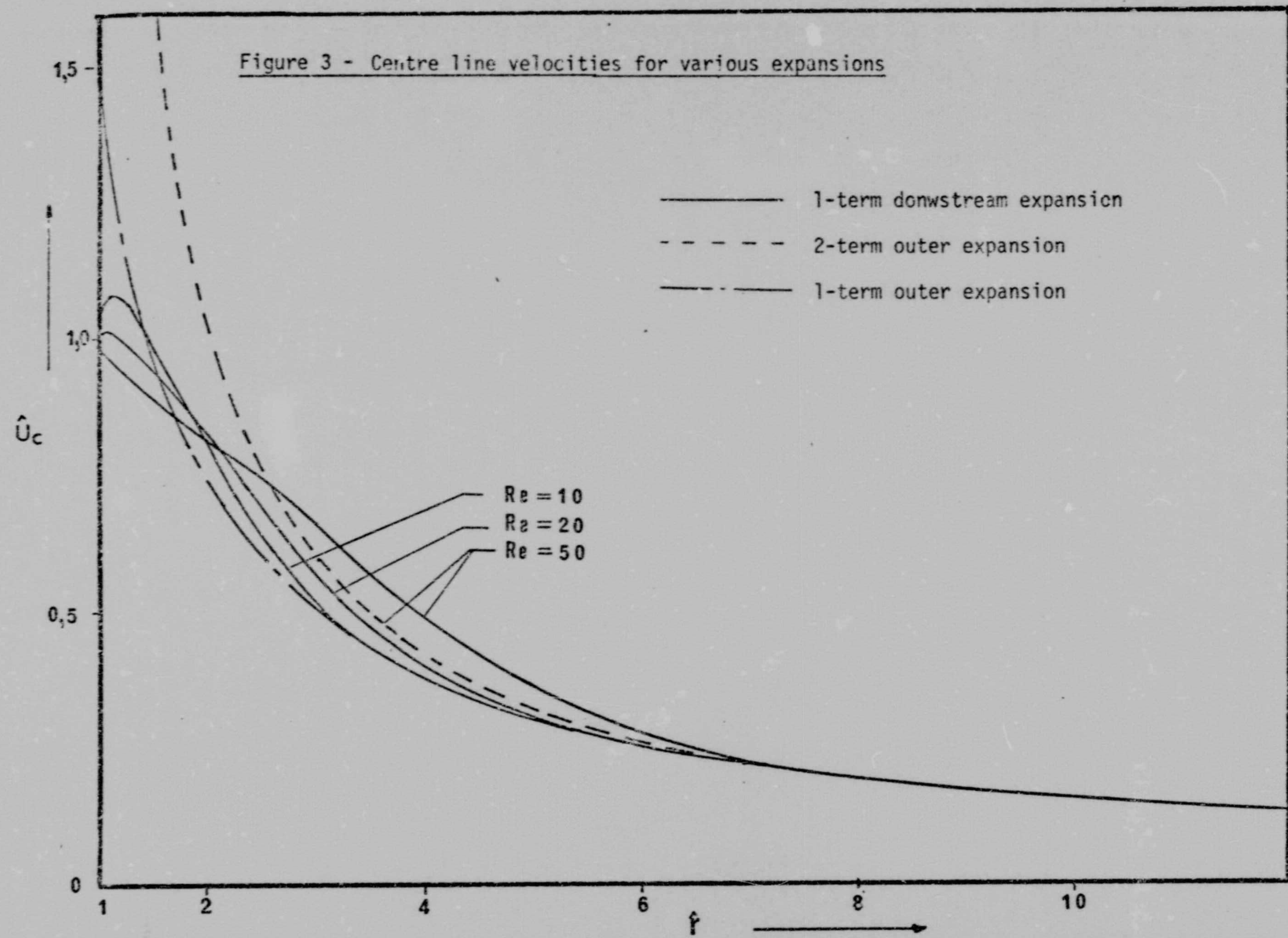

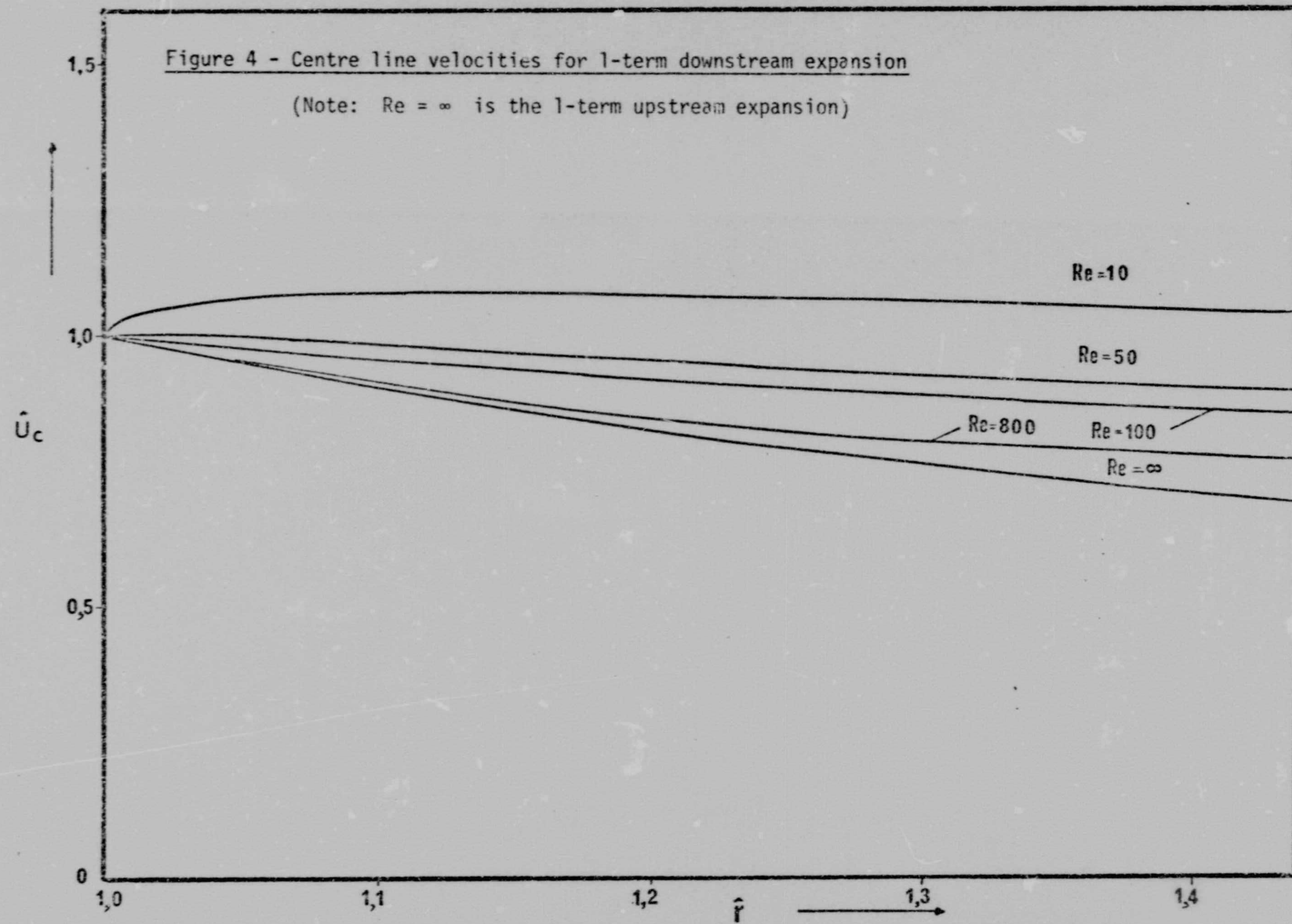


Figure 4 - Centre line velocities for 1-term downstream expansion

(Note: Re = ∞ is the 1-term upstream expansion)

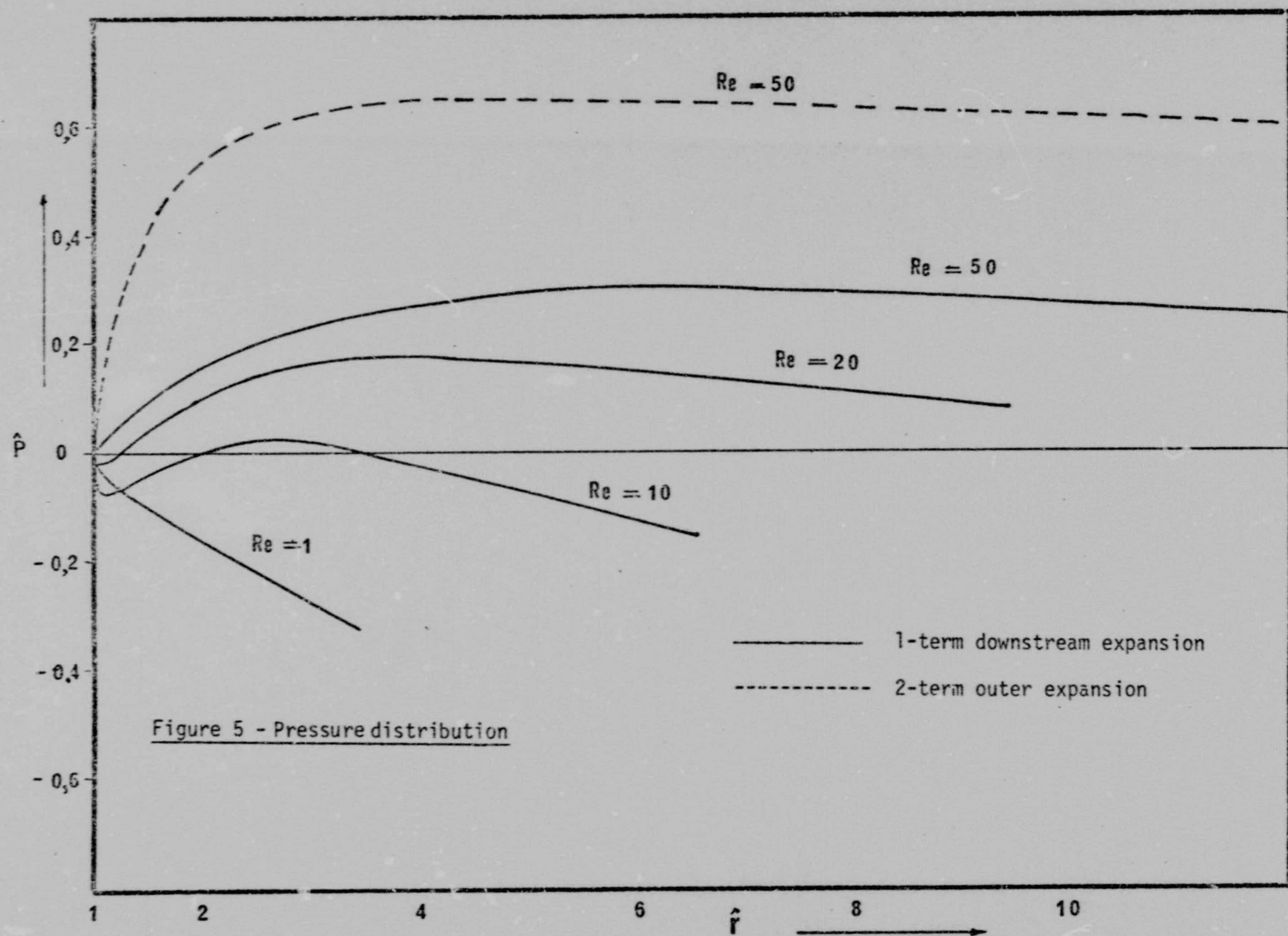


Figure 5 - Pressure distribution

the two-term outer expansion (region 3). For Re = 1 the pressure gradient is never zero and hence there are no points of inflexion in the velocity profile. For higher Reynolds numbers however, there are points of zero pressure gradient and in some cases two. This is a result of the relative magnitudes of the acceleration and deceleration effects. In all cases, the pressure distribution as determined from the downstream expansion is lower than that obtained from the outer expansion. This is in accordance with the experimental results of Jackson and Symmons (1965) who found that although Savages' (1964) solution gave the correct form for the pressure distribution, the experimental distributions were in most cases lower.

It can be seen from Figure 5 that the pressure gradient becomes more and more unfavourable with increasing Reynolds numbers. This means that at some critical Reynolds number the fluid in the channel will be unable to overcome the unfavourable pressure gradient and separation must then occur. Since this is a confined flow problem the outer flow, i.e. the centre core, will be accelerated (in order that continuity be obeyed) which in turn will tend to reduce the unfavourable pressure gradient and the flow will then, when the pressure gradient is sufficiently reduced, reattach further downstream.

In the present study it was found that for Re $\geqslant$ 60 separation occurred. As the Reynolds number was increased, the separation point moved upstream while the reattachment point moved downstream and in the limit, i.e. Re $\to \infty$, the separation point tended towards that given by Görtler (1957) for diverging flow over a flat plate. Figure 6 is a plot of separation point versus Reynolds numbers. Since the numerical technique was stable for negative velocities it was possible to investigate the behaviour of the boundary layer solution at the separation point. In all cases studied the solution remained regular, no singular behaviour as described by Goldstein (1948),

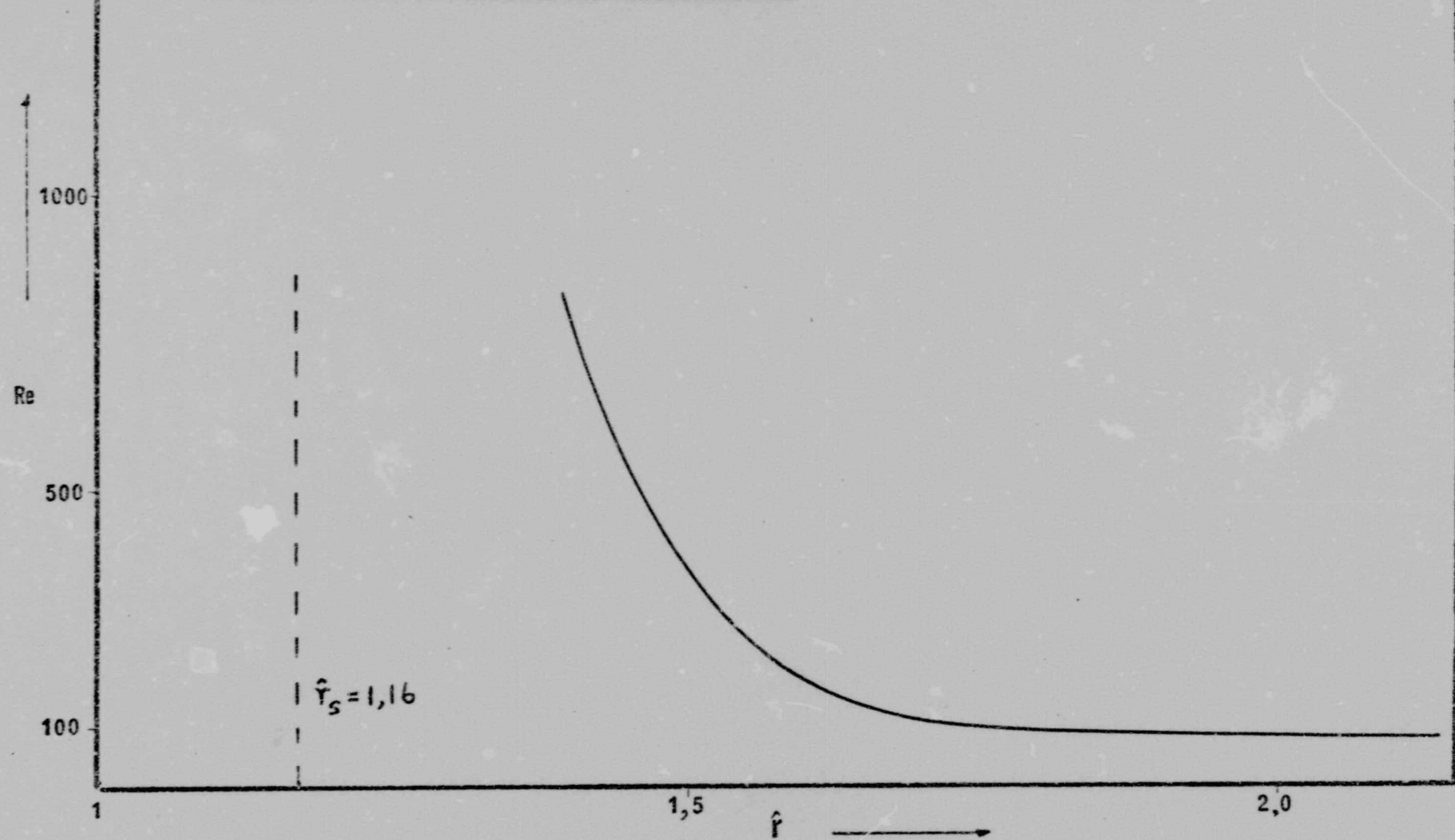


Fig. 6 - Separation point versus Reynolds number

Stewartson (1958) and Kaplun (1967) was observed. This is in fact in accordance with the work of Catherall and Mangler (1966) and Brown and Stewartson (1969) who have noticed that if the external flow field is not specified the separation point remains regular. In the numerical procedure used the pressure gradient was regarded as one of the unknowns and was then subsequently solved step by step in the marching process.

In Figure 7a we have plotted for Re = 100 the velocity profiles at various $\hat{z}$ against the radial co-ordinate. It can be seen that the separation bubble is confined to a small neighbourhood of the wall. Also depicted in Figure 7a is the radial pressure distribution, which has become slightly flattened in the region of the separation bubble. In Figure 7b we have shown the effect of separation on the downstream expansion: the centre line velocity still tends asymptotically towards the outer expansion. (Note the characteristic hump in the downstream velocity profile is due to the acceleration effect caused by the separation bubble.)

It is instructive at this stage to review some of the results of Ishizawa (1965). His method predicted that separation would not occur for Re < 100. Our analysis shows, however, that it is possible to get separation even for Reynolds numbers as low as 60. This discrepancy is attributed to the convergence problems of his series solution. Even at Re = 100 Ishizawa's series solution was unable to converge satisfactorily, and he was forced to extrapolate, using a numerical method of Görtler's (1948) which predicted the separation point to be at $\hat{r}_s = 1{,}770$. This is still in good agreement with our method which predicts separation, for Re = 100, at $\hat{r}_s = 1{,}7749$.

Furthermore, Ishizawa's (1965) method is based ultimately on that of Schlichting's (1960) which has been shown by van Dyke (1970) and Wilson (1971) to be incorrect; the displacement effect of the growing boundary layers induces a change in the inviscid core which near the entrance will not resemble a uniform core. In section 3.1 we have formulated the second order inviscid problem which takes displacement effects into account but because of the rather complicated boundary conditions it was not possible to find an analytic solution. However as shown in Figure 4, the

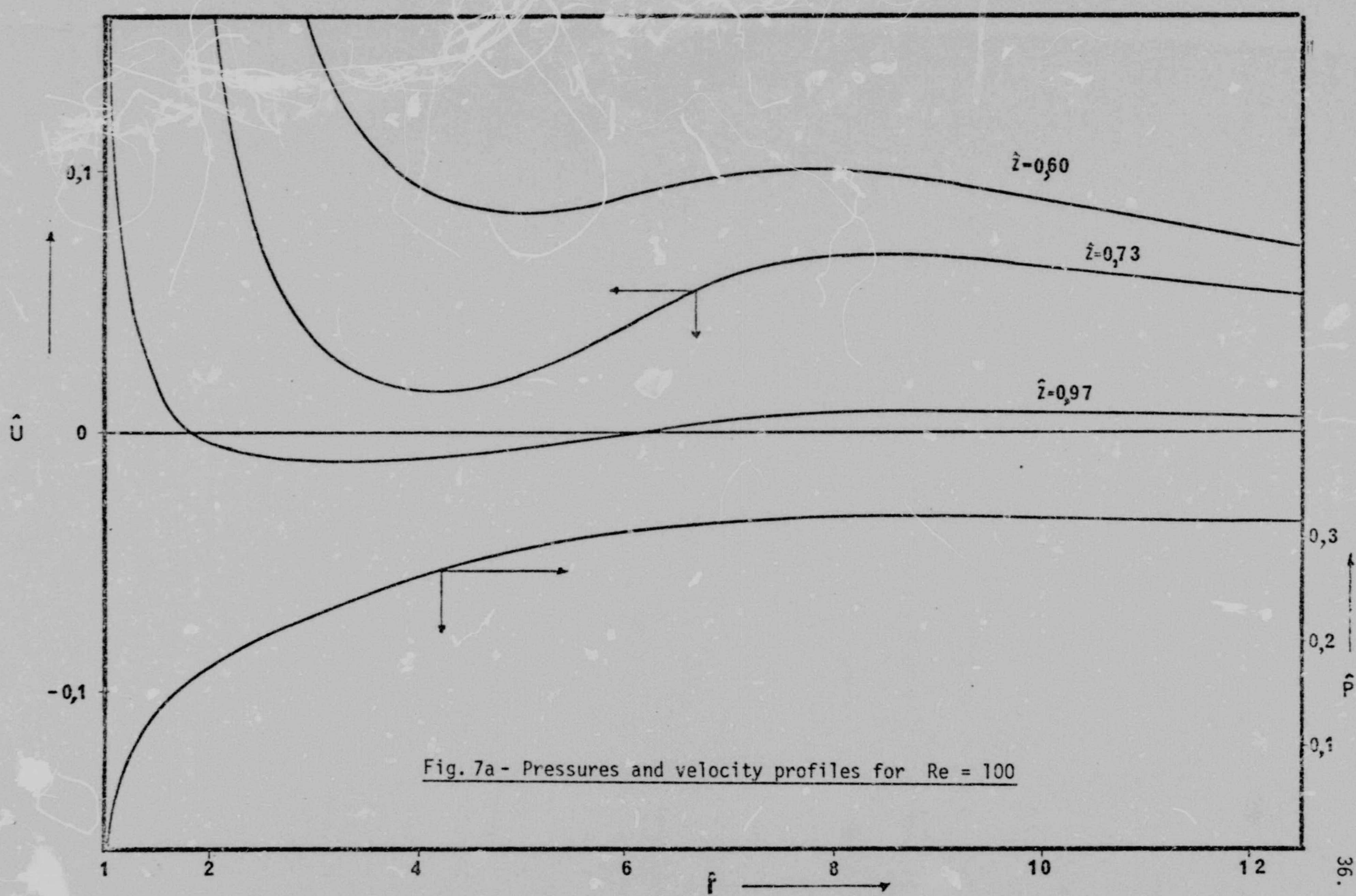


Fig. 7a - Pressures and velocity profiles for Re = 100

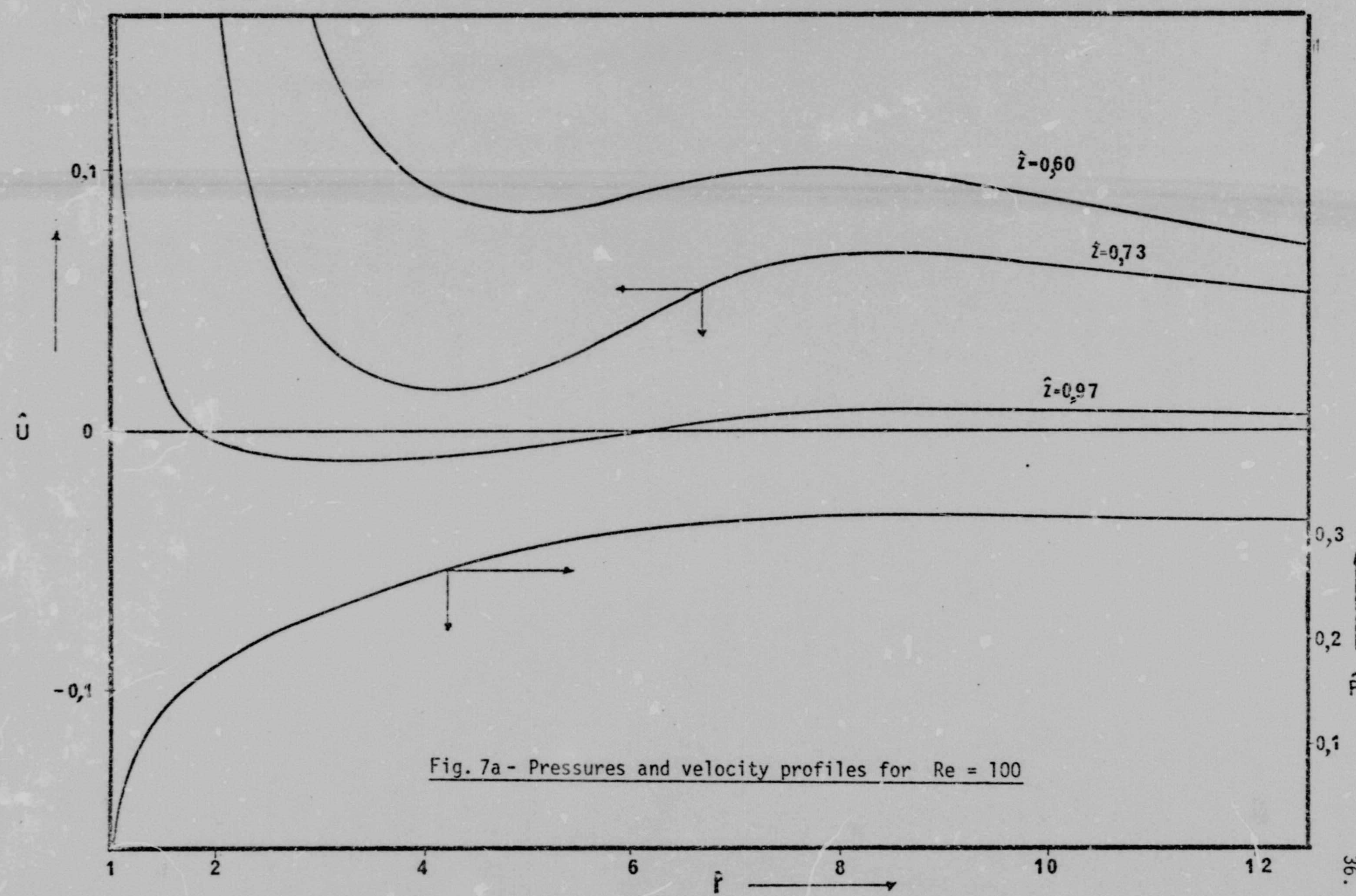


Fig. 7a - Pressures and velocity profiles for Re = 100

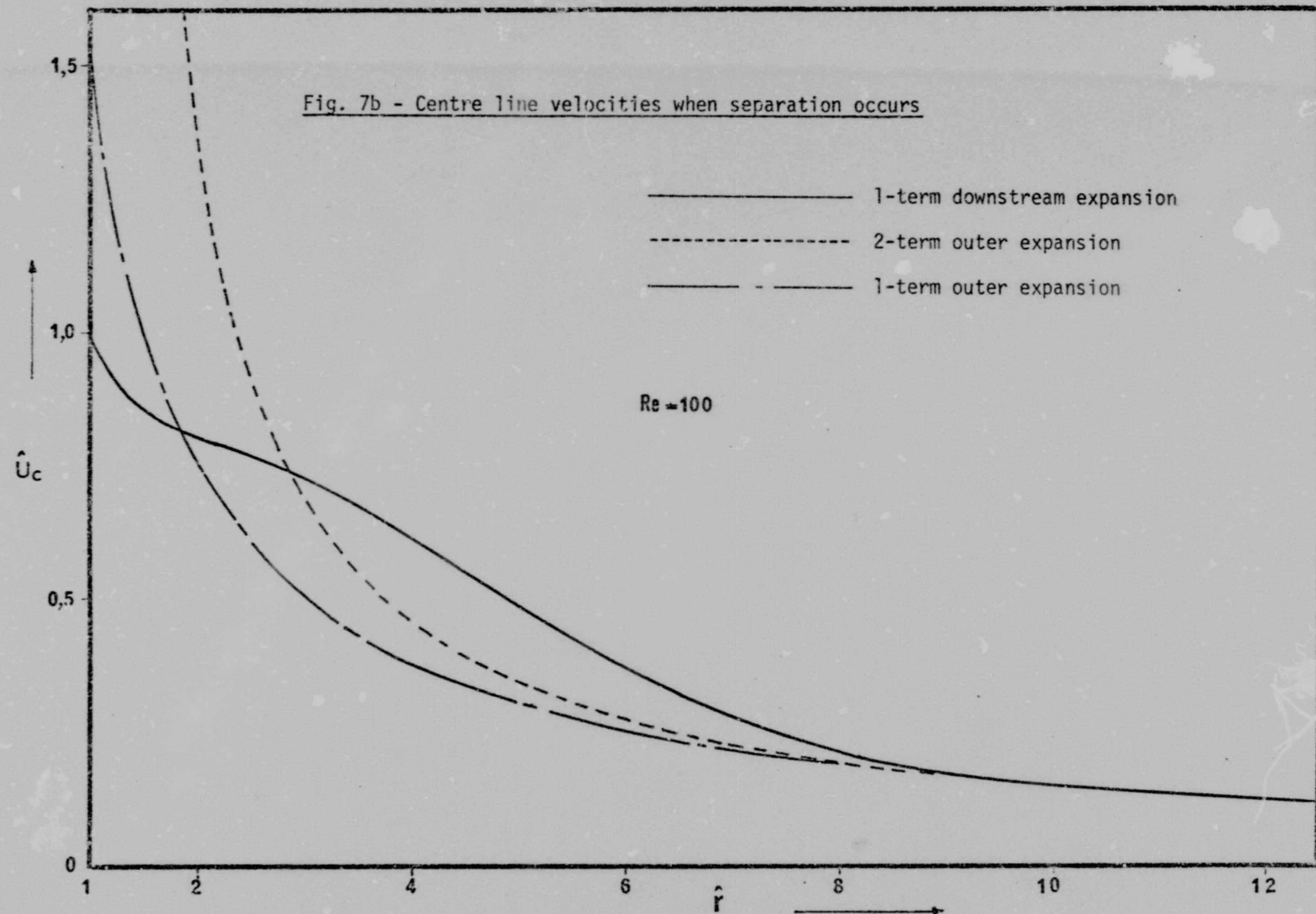


Fig. 7b - Centre line velocities when separation occurs displacement effect for large Reynolds numbers is extremely small and hence Ishizawa's analysis under these conditions may be sufficiently accurate to describe region 1 as well. This point, unfortunately, can only be clarified once the second order problem has been solved or else by solving the full Navier-Stokes equations, that is numerically.

Our analysis is based on specifying irrotational flow at some finite radius (see inlet boundary conditions (2-11)). Wilson (1971) and van Dyke (1970) have shown that if this is done for the parallel plate channel various mathematical difficulties are encountered. (A singularity occurs at the entrance and there is also the intrusion of fractional powers of the Reynolds number into the expansion.) They found that the most tractable and realistic model was one where no conditions were imposed at the channel entrance, i.e. the flow conditions are specified far upstream. For the parallel disk situation it is physically only possible to specify the inlet conditions at some finite $\hat{r}$ (due to the singularity at the origin) and our choice was therefore limited to either specifying a uniform profile or else a uniform profile with zero vorticity. We choose the latter since the analysis for the first order problem is then less complicated, but in any event we should expect certain mathematical difficulties with the second order problem.

An interesting result occurs if we rewrite our outer expansion in terms of Savage's (1964) variables; the expansion becomes

$$\hat{r}\hat{\phi} \sim F_0(\hat{z}) + \left(\frac{Re}{\hat{r}^2}\right)F_1(\hat{z}) + \left(\frac{Re}{\hat{r}^2}\right)^2 F_2(\hat{z}) + \ldots \qquad (3\text{-}41)$$

Comparing the above with Savage's expansion we notice that the first two terms are identical but the third term is of $O(Re/\hat{r}^2)^2$ while Savage's third term is of $O(\sqrt{Re}/\hat{r}^2)^2$. Furthermore the function $F_2(\hat{z})$ is not identical to Savage's. This is to be expected since unlike Savage's expansion, (3-39) is a parameter expansion and there is therefore no reason to believe that it should proceed in a similar manner. The fact that the first two terms are identical is fortuitous.

## 3.3 CONCLUSIONS

We have shown that if the variables are scaled correctly it is possible to reanalyse source flow between parallel disks in the limit of high Reynolds numbers, and in so doing are able to construct asymptotic expansions for various regions of the flow. Unlike Wilson (1972) and Savage (1964) these expansions are all of the parameter type and indeterminacy does not arise. The problem itself then reduces to an entry flow problem with three discernible regions. Regions 1 and 2 were remarkably similar to those found by van Dyke (1970) in his analysis of entry flow in a parallel plate channel, however there were some rather unique features.

Firstly, the scaling of the co-ordinate in the flow direction for the downstream region was of $O(Re^{\frac{1}{2}})$ instead of $O(Re)$. This is to be expected as the boundary layers develop under an adverse pressure gradient and will subsequently fill the channel much sooner. Secondly, the downstream expansion as a result of matching with the upstream expansion depended explicitly on the Reynolds number and separation effects could therefore be analysed. In all cases studied the separation points were found to be regular and for Reynolds numbers lower than 60, separation did not take place. For high Reynolds numbers it was possible to approximate regions 1 and 2 with a downstream expansion.

In region 3 the correct scaling for the radial co-ordinate was found to be $\rho = r/hRe$. The asymptotic expansion corresponding to this region is similar to Savage's (1964), i.e. the first two terms are identical, however higher order terms are different.

# 4. EXPERIMENTAL INVESTIGATION OF REVERSE TRANSITION

## 4.1 APPARATUS

To achieve radial flow, two perspex disks 300mm in diameter, 12,7mm thick were set up as in Figure 8. The fluid medium, air, entered through the bottom disk which was bolted to a rigid frame. To eliminate separation it was necessary to have a curved inlet on the bottom plate as well as a centre body attached to the top plate (see Figures 9 - 10); both were designed according to Moller (1966).

To ensure that the gap width was uniform, the inner surfaces of the disks were machined and then supported between each other with three spacers which were machined to ±0,025mm. The spacers were annular metal rings supported on a threaded rod. This enabled the disks to be bolted together. By using different spacers various gap widths could be obtained.

A centrifugal fan supplied the air and the flow rate was varied by decreasing or increasing the resistance of the air filter. The v[illegible]tric flow rate was measured using an orifice plate designed according to [illegible] American Society for Testing Materials. Since a wide range of flow rates were encountered two orifice plates were used to facilitate pressure drop readings. The pressure drop was measured with an inclined manometer which could read accurately to 0,005mm of water. To ensure that no vibrations from the fan were transmitted to the disks, two flexible couplings were placed on either side of the orifice plate.

In order to obtain some measure of the radial pressure distribution the top disk was pressure tapped at 10mm intervals along half a disk diameter.

The taps consisted of 0,5mm diameter holes which were bored out near the surface to 5,0mm. Perspex plugs were glued in place onto which flexible pressure tubes were attached. These tubes were connected to the inclined manometer.

The traversing mechanism can be conveniently described by referring to Figure 11. A 20mm wide 270mm long slot was milled out of the top disk (A) into which fitted a perspex slide (B). The sli[illegible] was carefully machined so that its bottom surface (D) was flush with the bottom surface (C) of the disk. The traversing mechanism consisted of two perspex blocks (F) and (G) which were held together by a finely threaded screw (H) which was fixed but free to rotate in (G) and threaded in (F). This allowed the top block (F) to move relative to the bottom block (G).